Noise Modeling and Measurement Techniques

ALAIN CAPPY

(*Invited Paper*)

Abstract—**The HEMT noise behavior is presented from theoretical and experimental points of view. The general method used in the high-frequency noise analysis is described and the different approximations commonly used in the derivation of the noise parameter expressions are discussed. A comparison between the noise performance of both MESFET's and HEMT's is carried out. The measurement techniques providing the noise figure and the other noise parameters are then described and compared.**

I. Introduction

DURING THE PAST five years, the high electron mobility transistors (HEMT, also called TEGFET, MODFET, SDHT $\cdots$) employing modulation-doped AlGaAs/GaAs heterostructures has demonstrated excellent performance in the field of microwave amplifiers [1], [3]. Recently, a small-signal gain of 3.6 dB and an output power of 3.4 mW with 2 dB gain have been reported at 94 GHz for a single-stage amplifier [4]. Moreover HEMT devices capable of a noise figure as low as 2.7 dB at 62 GHz with 3.8 dB associated gain have been successfully produced. More generally, Fig. 1 shows the reported HEMT noise performance at room temperature from different laboratories. These performances are superior to those of conventional MESFET's, and the reasons of this superiority are interesting.

In the next section, the general method used in noise analysis is presented, including the calculation of the gate and drain noise sources and their correlation coefficient, as well as the calculation of the noise figure and the other noise parameters. The different approximations and assumptions commonly used in the noise figure derivation are discussed and the specific influence of the gate noise and of the correlation coefficient is emphasized. A comparison between the HEMT and MESFET noise performance is then carried out in order to illustrate the main reasons of the HEMT superiority in the fields of low-noise amplifiers. Results on the HEMT low-frequency noise behavior, an important parameter in oscillator spectral purity, are then presented. Different structures with reduced low-frequency noise are proposed. The last section reviews the high-frequency noise figure measurement techniques and gives their respective advantages and drawbacks, especially in terms of measurement accuracy.

Manuscript received May 4, 1987; revised July 27, 1987.

The author is with the Centre Hyperfréquences et Semiconducteurs, Université des Sciences et Techniques de Lille, 59655 Villeneuve d'Ascq Cedex, France

IEEE Log Number 8717580.

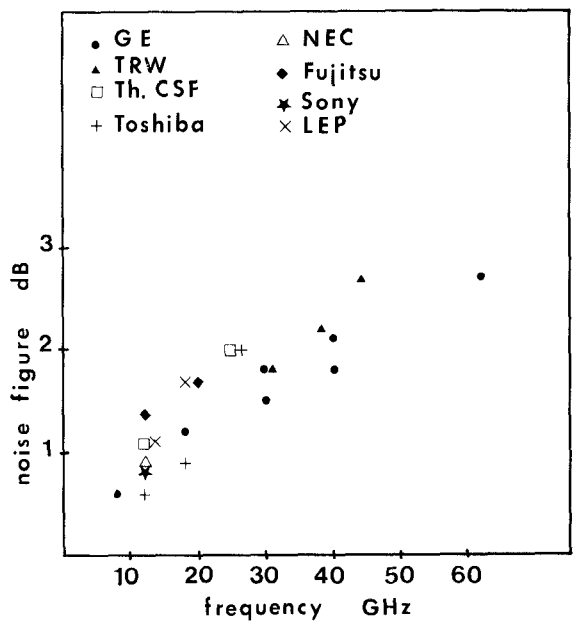

Fig. 1. Reported HEMT noise performance at room temperature.

II. High-Frequency Noise Modeling in HEMT's

From the point of view of the circuit designer, the noise performance of the HEMT is characterized by three noise parameters: the minimum noise figure $F_{\min}$, the noise conductance G_n (or noise resistance R_n), and the optimum source impedance Z_{opt} (or optimum source admittance Y_{opt}). These noise parameters can easily be calculated from the equivalent circuit of the noisy HEMT presented in Fig. 2(a). This circuit comprises the well-known small-signal equivalent circuit and the four noise sources $\overline{e_g^2}, \overline{e_s^2}, \overline{i_g^2}, \overline{i_d^2}$. The two noise sources $\overline{e_g^2}$ and $\overline{e_s^2}$ represent the noisy behavior of access resistances R_g and R_s and are simply given by the Nyquist formula

$$\overline{e_i^2} = 4kTR_i\Delta f \tag{1}$$

where k is the Boltzmann constant, T the absolute temperature, R_i the resistance value, and Δf the frequency bandwidth. The two current noise sources $\overline{i_g^2}$ and $\overline{i_d^2}$ represent the internal noise sources of the intrinsic HEMT. These noise sources are correlated.

By means of a simple circuit manipulation, these four noise sources are transformed in two correlated noise sources $\overline{v^2}$ and $\overline{i^2}$ preceding the extrinsic HEMT, which is

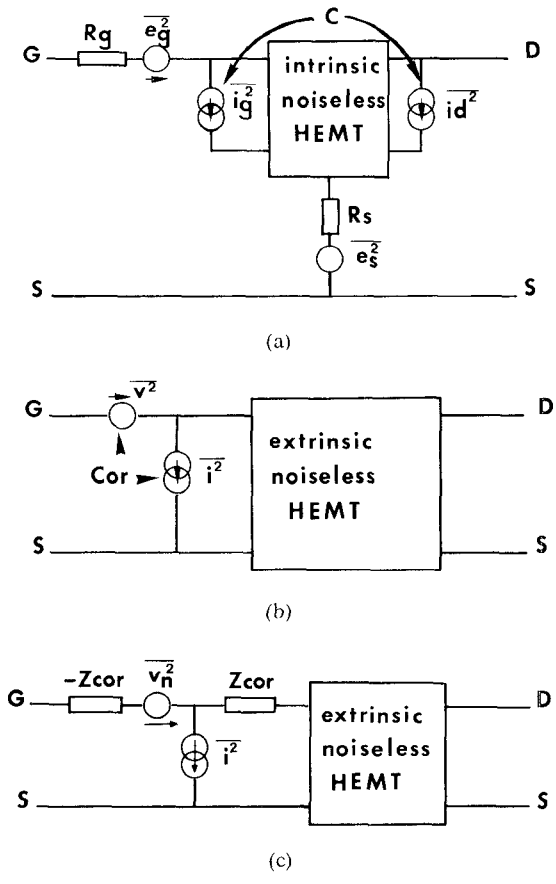

Fig. 2. Circuit transformations for the noise figure determination.

now considered noiseless (Fig. 2(b)). Lastly, $\overline{v^2}$ and $\overline{i^2}$ are decorrelated by introduction of two (noiseless) correlation impedances (Fig. 2(c)). At this step, the calculation of $F_{\min}$ and Z_{opt} is straightforward and gives

$$F_{\min} = 1 + 2g_n(R_{\text{cor}} + R_{\text{opt}}) \tag{2}$$

where

$$Z_{\text{cor}} = R_{\text{cor}} + jX_{\text{cor}} \qquad g_n = \overline{i^2}/4kT\Delta f$$
$$r_n = \overline{v_n^2}/4kT\Delta f$$

and

$$Z_{\text{opt}} = R_{\text{opt}} + jX_{\text{opt}} = \sqrt{R_{\text{cor}}^2 + \frac{r_n}{g_n}} - jX_{\text{cor}}.$$

More details of this noise figure calculation technique can be found in [1] and [2].

This synopsis of the noise analysis shows that the determination of the HEMT's noise performance requires (i) knowledge of the small-signal equivalent circuit and (ii) the gate and drain noise sources $\overline{i_g^2}$ and $\overline{i_d^2}$, as well as their correlation coefficient, defined by

$$C = \frac{\overline{i_g i_d^*}}{\sqrt{\overline{i_g^2}\cdot\overline{i_d^2}}}. \tag{3}$$

Therefore, a noise modeling will be divided into two steps: the calculation of the small-signal equivalent circuit and the calculation of the noise sources $\overline{i_g^2}, \overline{i_d^2}$ and the correlation coefficient C. In fact, the method used for the noise source calculation [3]–[5] is usually derived from the Shockley impedance field method and it may be appropriate to recall briefly the principles of this method.

In the microwave frequency range, the noise arises from the fluctuation of carrier velocity due to the scatterings with phonons or ionized impurities. In a section of the HEMT channel (length dx, width Z, sheet carrier density $N(x)$), the local noise current can be expressed as [6]

$$\overline{i_d^2(x)} = q^2 ZN(x)\overline{\Delta v_{\parallel}^2}/dx. \tag{4}$$

In this expression $\overline{\Delta v_{\parallel}^2}$ represents the mean square of the velocity fluctuations. In the microwave frequency range, the spectrum of $\overline{\Delta v_{\parallel}^2}$ is white, leading to a local noise current spectral density given by

$$Si_d(x) = 4q^2 ZN(x)D_{\parallel}(x)/dx \tag{5}$$

where $D_{\parallel}(x)$ is the diffusion coefficient parallel to the electrical field direction. This expression is quite general and can be applied for a resistance at thermal equilibrium (thermal noise) and/or for the high field region of the HEMT channel (diffusion noise).

The purpose of the impedance field method is to determine the effects of the *local* noise sources $Si_d(x)\cdot\Delta f$ on the drain and gate electrodes. The device noise behavior will then be entirely characterized by two correlated equivalent gate and drain noise sources. Let $Z(x,\omega)$ be the small-signal impedance between the abscissa x and the drain electrode. The drain voltage fluctuation $\overline{v_d^2(x)}$ arising from the local noise source located between x and $x + dx$ is given by

$$\overline{v_d^2(x)} = 4q^2 ZN(x)D_{\parallel}(x)\left|\frac{dZ(x,\omega)}{dx}\right|^2 \Delta f\cdot dx. \tag{6}$$

Assuming that the noise current sources located at two different abscissas x and x' are uncorrelated, the open-circuit noise voltage $\overline{v_d^2}$ is given by a summation performed over the whole length of the active channel.

$$\overline{v_d^2} = \int 4q^2 ZN(x)D_{\parallel}(x)\Delta f\left|\frac{dZ(x,\omega)}{dx}\right|^2 dx. \tag{7}$$

It is then convenient to define the short-circuit noise current $\overline{i_d^2}$ by $\overline{i_d^2} = |y_{22}|^2\overline{v_d^2}$, where y_{22} is an intrinsic admittance matrix parameter defined by $\underline{y}_{22} = g_d + j\omega C_{gd}$.

The gate noise current source $\overline{i_g^2}$ and the correlation coefficient C are calculated in a similar way [5], [6], and can be expressed as

$$\overline{i_g^2} = 4q^2 Z\Delta f\omega^2 \int N(x)D_{\parallel}(x)\left|\frac{d}{dx}\left(\frac{\partial Q(x)}{\partial I}\right)\right|^2 dx \tag{8}$$

$$\overline{i_g i_d^*} = j\omega 4q^2 Z\Delta f\int N(x)D_{\parallel}(x)\left(\frac{d}{dx}Z(x,\omega)\right)\cdot\left(\frac{d}{dx}\left(\frac{\partial Q(x)}{\partial I}\right)\right)dx. \tag{9}$$

In these expressions, Q is the total amount of stored

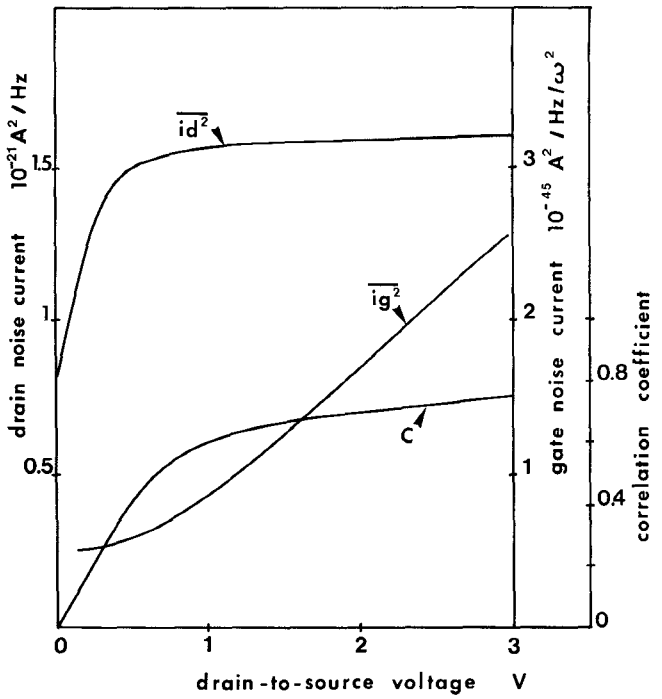

Fig. 3 Evolution of the drain and gate noise current sources and the correlation coefficient versus V_{ds}, $V_{gs} = -0.5$ V, $L_g = 0.5$ μm, $A = 500$ Å, $N_d = 10^{18}$ cm^{-3}

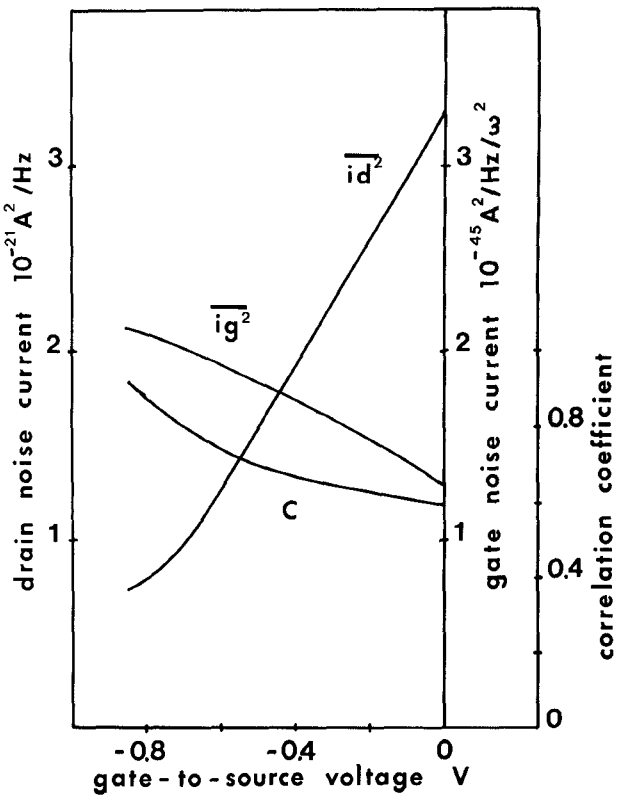

Fig. 4. Evolution of the drain and gate noise current sources and of the correlation coefficient versus V_{gs}. $V_{ds} = 2$ V, $L_g = 0.5$ μm, $A = 500$ Å, $N_d = 10^{18}$ cm^{-3}.

charge in the device and therefore $\partial Q(x)/\partial I$ represents the stored charge fluctuation induced by a local noise source. Expressions (7), (8), and (9) show that the calculation of the HEMT noise performance requires, for each section of the channel, the sheet carrier density $N(x)$, the diffusion coefficient $D_{\|}(x)$, and the impedance and "charge" fields dZ/dx and $d/dx(\partial Q/\partial I)$. Since $N(x)$ is given by the dc drain current $I_{ds} = qZN(x)v(x)$, and $D_{\|}(x)$ is assumed to be dependent on the local electrical field [4] or local average energy [5], the main problem encountered in noise modeling is to calculate the impedance and "charge" fields. According to the type of modeling, this can be done in an analytical [3], [4] or a numerical form [6].

It should be emphasized that the impedance field method applies only to 1-D modeling, at least in its classical form. In most cases, the device noise properties are thus calculated *below* the onset of saturation [8]–[10], which obviously constitutes an important approximation.

It should be also noted that other techniques can be used for the noise analysis. As a matter of fact, statistical procedures, such as 2-D Monte Carlo modeling, provide the instantaneous current $I(t)$ and consequently the mean square current fluctuations $\overline{\Delta I^2(t)} = \overline{(I(t) - \bar{I})^2}$. The noise current spectral density can be easily deduced from $\overline{\Delta I^2(t)}$ by a Fourier transform [10]. However, since very long time periods cannot be studied by a 2-D Monte Carlo procedure, the results of such a method concern mainly the device noise behavior in the millimeter-wave range. Unfortunately, this method has not been applied for the HEMT case yet.

Returning to the noise source calculation problem it seems appropriate at this step to discuss the evolution as a function of the gate and drain bias voltages. For this purpose, Fig. 3 shows the evolutions of both the noise current sources $\overline{i_d^2}$ and $\overline{i_g^2}$, and the correlation coefficient C versus V_{ds} for a given V_{gs}. These results have been obtained using the numerical noise modeling of Cappy *et al.* [5], which takes the nonstationary electron dynamics and the carrier injection into the buffer into account. This figure shows that $\overline{i_d^2}$ and C increase in the ohmic region and tend to saturate at high drain voltage, while $\overline{i_g^2}$ increases with a near constant slope versus V_{ds}. This indicates that the hot electron effects, which are more pronounced at high V_{ds}, affect mainly the gate noise and, to a lesser extent, the correlation coefficient.

As a function of V_{gs}, Fig. 4 shows a strong decrease of $\overline{i_d^2}$ and an increase of both $\overline{i_g^2}$ and C as the dc drain current diminishes.

When the noise sources are known, the problem is to calculate the noise figure and the other noise parameters. Due to the large number of different parameters influencing the noise figure, a physical analysis of the noise properties is rather difficult in the most general case. For this reason, it is convenient to introduce the different elements step by step in order to make their influence easier to understand.

III. The Noise Parameters

In a first approximation, the gate noise source $\overline{i_g^2}$ and feedback capacitance C_{gd} can be neglected. Following van der Ziel [7], [8], the drain noise source $\overline{i_d^2}$ can be

expressed as

$$\overline{i_d^2} = 4kTg_m P\Delta f \tag{10}$$

where g_m is the transconductance and P is a dimensionless parameter close to 1–3, depending upon the technological parameters and biasing conditions. Introducing expression (10) in the noise figure calculation yields

$$F_{\min} = 1 + 2\sqrt{P} \cdot \frac{f}{f_c} \cdot \sqrt{g_m(R_s + R_g)} \tag{11}$$

$$g_n = Pg_m(f/f_c)^2 \tag{12}$$

$$Z_{\text{opt}} = \sqrt{\frac{g_m(R_s + R_g)}{P}} \cdot \frac{1}{C_{gs}\omega} + \frac{1}{jC_{gs}\omega} \tag{13}$$

where $F_{\min}$ is the minimum noise figure, g_n the noise conductance, Z_{opt} the optimum input impedance, and f_c is the cutoff frequency $g_m/2\pi\ C_{gs}$. It can be noted that expression (11) is similar to the well-known and widely used Fukui formula, where the so-called fitting factor kf is given by $2\sqrt{P}$. Classically, expression (11) shows that a low $F_{\min}$ value requires a high f_c and small values of both the sum $R_s + R_g$ and the coefficient P. In fact, the P value greatly influences $F_{\min}$, g_n, and Z_{opt} and its determination is obviously of primary importance.

According to Delagebeaudeuf [9], the parameter P can be approximated for operating points below the onset of saturation by

$$P = \frac{I_{ds}}{E_c L_g g_m}. \tag{14}$$

In this expression I_{ds} is the dc drain current, E_c the critical field of an idealized $v-E$ relationship, L_g the gate length, and g_m the transconductance.

Usually the transconductance of HEMT's is higher than that of conventional MESFET's. Therefore the coefficient P and, of course, the Fukui fitting factor $kf = 2\sqrt{P}$ is lower for HEMT's. Introducing (14) in (11) yields

$$F_{\min} = 1 + 2\sqrt{\frac{I_{DS}}{E_c L_g}} \cdot \frac{f}{f_c} \cdot \sqrt{R_s + R_g}. \tag{15}$$

It should be emphasized that, as far as the design of low-noise devices is concerned, expressions (15) and (11) yield quite different conclusions. Indeed, following (11), for a given gate length and therefore a near constant cutoff frequency f_c, the noise figure can be reduced by reducing the transconductance g_m. In other words, the noise figure can be improved using a large epilayer thickness. On the contrary, the transconductance is no longer present in expression (15) and the preceding conclusion does not hold. From an experimental point of view, it is rather difficult to separate these two approaches. For this purpose, Table I presents different reported results. These results show that very high transconductance can provide a low noise figure (device I). Furthermore, with similar gate length, access resistance value, and cutoff frequency, device V [large epilayer thickness (570 Å) and rather low g_m (220 mS/mm)] and device VI [400 Å epilayer thickness and higher g_m (275 mS/mm)] exhibit similar noise performance. It should be also noted that the kf factor deduced from experimental findings varies significantly from one device to another. For the data of Table I, kf varies from 1.2 to 2.5 without any obvious correlation with the other device parameters.

The important problem encountered in the comparison between the expressions (11) and (15) of the noise figure probably arises from the assumptions used to deduce these formulas. In particular, it seems important to consider the influence of the gate noise source and the correlation coefficient. According to the pioneering work of van der Ziel [8], the gate noise current source $\overline{i_g^2}$ can be expressed as

$$\overline{i_g^2} = 4kT\Delta f C_{gs}^2 \omega^2 R/g_m \tag{16}$$

where R is a dimensionless multiplication parameter depending upon biasing conditions and device parameters. Neglecting the influence of C_{gd}, the calculation of $F_{\min}$ and other noise parameters can be carried out analytically and yields

$$F_{\min} = 1 + 2\sqrt{P + R - 2C\sqrt{PR}} \cdot \frac{f}{f_C} \cdot \sqrt{g_m(R_s + R_g) + \frac{PR(1-C^2)}{R + P - 2C\sqrt{RP}}} \tag{17}$$

$$g_n = g_m\left(\frac{f}{f_c}\right)^2 \cdot \sqrt{P + R - 2C\sqrt{RP}} \tag{18}$$

$$Z_{\text{opt}} = \sqrt{\frac{g_m(R_s + R_g) + \frac{PR(1-C^2)}{P + R - 2C\sqrt{RP}}}{P + R - 2C\sqrt{PR}}} \cdot \frac{1}{C_{gs}\omega} + \frac{1}{jC_{gs}\omega} \cdot \left(\frac{P - C\sqrt{RP}}{P + R - 2C\sqrt{PR}}\right). \tag{19}$$

These expressions, like those obtained by Pucel [2], show different fundamental effects:

(i) The gate noise influences the noise figure *even at low frequency*.

(ii) The noise figure (in linear scale, not in dB) keeps a linear variation versus frequency even if the gate noise is taken into account.

(iii) If $R_s + R_g$ tends to zero, the noise figure is no longer close to unity if the gate noise is taken into account and the device can be characterized by an intrinsic noise figure:

$$F_{\text{int}} = 1 + 2\frac{f}{f_c} \cdot \sqrt{PR(1-C^2)} \tag{20}$$

(iv) Due to the correlation between the drain and gate noise current sources, the gate noise is partially subtracted from the drain noise. This important effect is expressed in the noise parameter expressions by the terms $P + R - 2\sqrt{PR}$ and $PR(1-C^2)$. This reduction of the drain noise

TABLE I

device	I	II	III	IV	V	VI	VII	VIII
ref.	[14]	[39]	[40]	[41]	[42]	[43]	[44]	[45]
geometry	0,25x150	0,35x65	0,35x62	0,4x200	0,5x200	0,5x200	0,5x200	0,55x200
gm mS/mm	570	230	330	250	220	275	235	290
gd mS/mm	32	23	17	18	15	20	15	20
Cgs pF/mm	1.8	0.95	2.05	1.0	1.2	1.25	1.3	1.2
Cgd fF/mm	100	230	78	100	50	100	50	165
Rg Ω	0,9	2.4	1.6	4	2.1	1	1	2
Rs Ω.mm	0,5	0,38	0,19	0,7	0,65	0,68	0,8	0,7
Fc GHz	50	38	26	40	29	35	29	38
fo,GHz	50	16	35	28	48	35	48	20
Fmin-dB 12 GHz	0,83	1.05	1.1	0,95	0,95	0,85	1.4	1.2
Gass dB	–	–	13	11,8	10,3	12,5	11	11
kf	1.43	2.5	2	1.33	1.2	1.28	1.9	1.8
Fcalc P=1,R=0.5 C=0.9	0.8	1.2	1.2	1.0	1.2	1.0	1.2	1.0
Fint calc P=1,R=0.5 C=0.9	0.6	0.77	1.08	0.73	0.98	0.83	0.98	0.77

is the basic reason why the field effect transistor (conventional or not) is a low-noise device. Therefore, it is not obvious to neglect the gate noise and the correlation coefficient in FET noise analysis.

From a theoretical point of view, the problem is to estimate the multiplication coefficient R and the correlation coefficient C. In fact, several papers [8], [11], [12] have shown that R (in MESFET's) is close to 0.2–0.4 below the onset of saturation. This is not negligible compared with the P value (close to 0.6–2) given by the same modeling. Independently and using a completely different approach, Cappy and coworkers have found R close to 0.5 and P close to 1–1.5 for the low-noise operating conditions (I_{ds} #100 mA/mm, $V_{ds} = 3$V). More precisely, Figs. 5 and 6 show the evolution of P, R, and C as a function of V_{ds} and V_{gs} for the same device parameters as for Figs. 3 and 4.

Concerning the correlation coefficient, which is one of the main parameters influencing the intrinsic noise figure, Fig. 4 shows that this parameter is strongly underestimated when the calculation is performed below the onset of saturation. Under low-noise conditions and for an operating frequency up to 20 GHz for a half-micron gate length

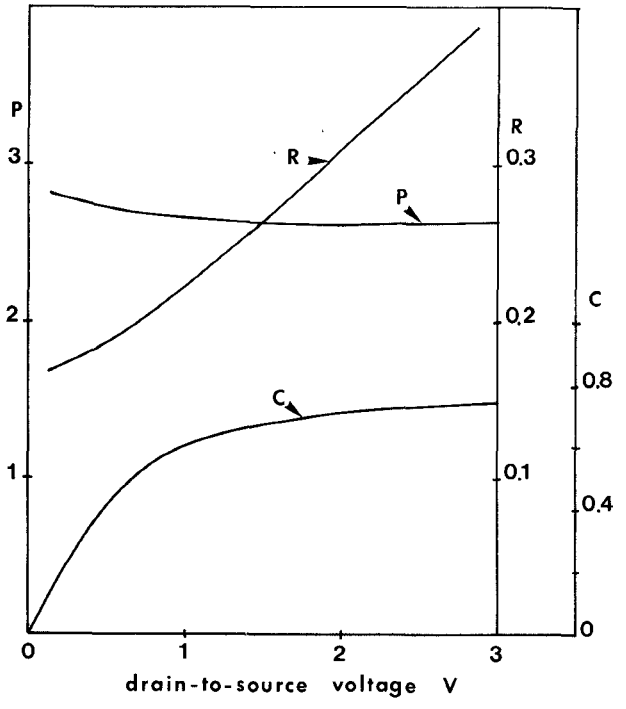

Fig. 5. Evolution of R, P, and C versus V_{ds}. $V_g = -0.5$ V.

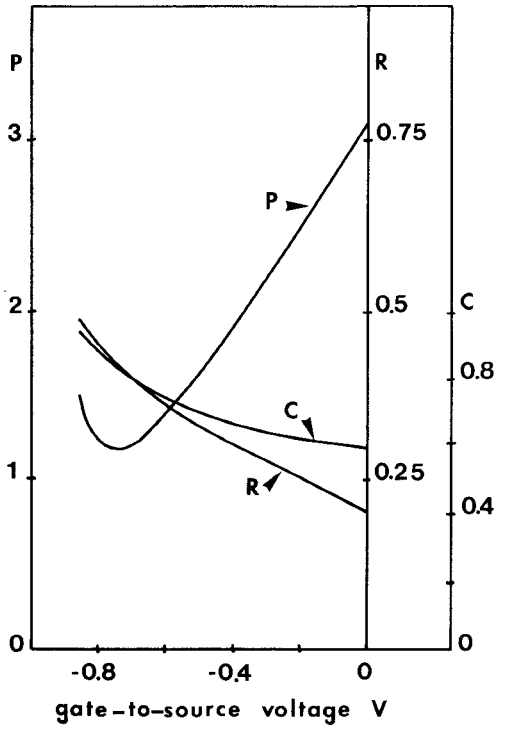

Fig. 6. Evolution of R, P, and C versus V_{gs}. $V_{ds} = 2$ V.

HEMT, C is practically purely imaginary and is close to 0.8–0.95. In addition, it seems that this parameter mainly depends on the aspect ratio L_g/A [5].

In order to show the validity of expression (17), both the extrinsic and intrinsic noise figures have been calculated for the different devices described in Table I. For this comparison, the same typical values of P, R, and C have been introduced in each case: $P = 1$, $R = 0.5$, $C = 0.9$. It should be noted that theoretical and experimental noise figures are now in good agreement. In addition, the important contribution of the intrinsic noise figure to the extrinsic noise figure should be pointed out.

IV. Influence of the Feedback Capacitance C_{gd}

In the preceding theoretical approaches, the feedback capacitance C_{gd} is neglected, which constitutes a strong approximation, especially for the noise figure derivation in the millimeter-wave range. The main influence of the gate-to-drain coupling is to make the drain noise current source frequency dependent, following the expression [5]

$$\overline{i_d^2} = \overline{i_{d_0}^2}\left(1 + \left(\frac{f}{f_0}\right)^2\right) \tag{21}$$

where $f_0 = g_d/2\pi C_{gd}$ and $\overline{i_{d_0}^2}$ is the drain noise source when C_{gd} is neglected. As a consequence, the noise figure rises steeper than the f law for frequencies beyond f_0. Furthermore, due to the evolution of g_d and C_{gd} versus V_{gs}, f_0 decreases for decreasing drain currents; consequently the optimum dc drain current increases with increasing operating frequency. These two effects have been found experimentally in the case of conventional MESFET's [13] and HEMT's [14].

The cutoff frequency f_0 constitutes an important parameter of the noise behavior of HEMT's; therefore, since a low output conductance is required for achieving high power gain, a reduction of C_{gd} is necessary in order to provide f_0 values as high as possible. From the experimental datas of Table I, f_0 is shown to be close to or greater than f_c except for devices II and VIII.

V. Comparison between MESFET's and HEMT's Noise Performance

A. The Noise Figure

The preceding noise analysis shows that the main parameters influencing the noise figure are the cutoff frequency f_c, the three noise parameters P, R, and C, and the sum of access resistances $R_s + R_g$.

Usually the cutoff frequency of HEMT's is larger than that of MESFET's for two main reasons:

(i) The high carrier mobility provides a more important overshoot effect, resulting in a higher average velocity and therefore a higher transconductance.

(ii) The small epilayer thickness yields high g_m, high intrinsic gate capacitance, and therefore a relatively less important effect of the parasitic capacitances.

Thus, the cutoff frequency of a typical 0.4–0.5 μm gate length HEMT is only slightly lower than that of the best 0.2–0.25 μm gate length conventional MESFET's [15], [16], which constitutes an important element of the HEMT superiority.

Concerning the noise coefficient P, R, and C, the situation is less clear since these parameters cannot be accurately provided by experiments and are mainly the results of theoretical considerations. Fortunately, for a given drain current, these parameters do not vary in a large extent, R is always close to 0.5–0.7 under low noise conditions while C mainly depends on the aspect ratio L_g/A. For short-gate-length MESFET's, C is close to 0.7–0.8 while a higher L_g/A ratio in the case of HEMT's provides a higher C value, close to 0.8–0.95.

In the case of the drain noise coefficient P, the difference between MESFET's and HEMT's is not important because of antagonistic effects, namely slight increases of P, firstly with increasing mobility and secondly with increasing epilayer thickness. The first effect arises from the relation between the low field diffusion coefficient and the carrier mobility (Einstein relation):

$$D_0 = \frac{kT}{q}\mu_0. \tag{22}$$

This relation holds for HEMT's and MESFET's at low electrical field strengths. For higher fields, theoretical works [7] have shown that the diffusion coefficient in a 2-D electron gas is similar to the bulk diffusion coefficient. Therefore, since the greater part of drain noise arises from the low field region [8], an increase of both $\overline{i_d^2}$ and P with increasing mobility is not surprising. Nevertheless, this effect is compensated in HEMT's by the decrease of P with decreasing epilayer thickness, and finally no im-

portant superiority of HEMT's over MESFET's arising from the noise coefficient P can be expected.

The last parameters determining the noise figure involve the sum of access resistances $R_s + R_g$. Since the gate resistance is dependent only on the gate fabrication process and device layout, the main problem arises from the source resistance. Furthermore, the choice of smaller gate width for increasing frequency operation involves a reduction of R_g, which becomes far less significant than the increasing value of access resistance R_s.

In the case of MESFET's, the source resistance R_s can be properly calculated from a knowledge of the active layer structure [18]. In the case of HEMT's, the source-to-gate access region is more complex and the source resistance value results from the conduction in several layers: the highly doped cap layer, the highly doped AlGaAs layer, and the 2-D gas [19], [20]. The complexity of the source–gate access involves several effects:

(i) The conventional transmission line method underestimates the parasitic source resistance [19].

(ii) Due to the capacitive effect of the depleted region at the AlGaAs/GaAs interface, the source resistance is frequency dependent [21].

Therefore, a precise determination of R_s is not obvious, especially at a high frequency of operation, yielding some difficulties in the correlation between the noise figure and the source resistance value. Nevertheless, very low values of both contact resistance ($R_c = 0.03\ \Omega\cdot$mm) and total access resistance ($R_s = 0.5\ \Omega\cdot$mm) have been achieved [22]. These results are comparable to the state-of-the-art of MESFET source resistances, and these two devices can be considered as equivalent as far as the parasitic resistances are concerned.

B. The Noise Conductance

In several applications such as broad-band amplifiers, the device is not matched for the minimum noise figure and the mismatch effect can be expressed as

$$F = F_{\min} + \frac{g_n}{R_0}|Z_0 - Z_{\text{opt}}|^2 \tag{23}$$

where $F_{\min}$ is the minimum noise figure, g_n the noise conductance, $Z_0 = R_0 + jX_0$ the input termination, or source, impedance, and Z_{opt} the optimum source impedance. This expression shows that the mismatch effect is less important for low values of the noise conductance g_n. As shown in expressions (12) and (18), the noise conductance is inversely proportional to the square of the cutoff frequency f_c. Since HEMT's exhibit a higher f_c value than MESFET's, HEMT's have lower noise conductance, which results in reduced sensitivity of the noise figure to changes in source impedance and therefore permits low-noise performance over a wider bandwidth. This effect has been experimentally shown by Pospieszalski *et al.* [23].

To summarize, the superiority of HEMT noise performance can be related to the higher cutoff frequency f_c and to the higher correlation coefficient reducing the intrinsic noise figure F_{int}, which represents, at least for the good devices having low access resistance values, an important part of the extrinsic noise figure $F_{\min}$.

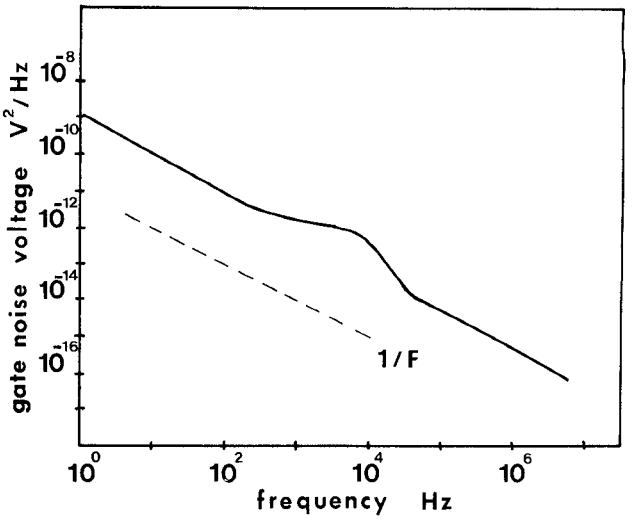

Fig. 7. Typical HEMT equivalent gate LF noise spectra.

VI. Low-Frequency Noise in HEMT's

In the preceding section, our attention was focused on the HEMT noise properties in the microwave frequency range. However, low-frequency (LF) noise is an important parameter in some applications, e.g. local oscillators, because the LF noise is up-converted in the microwave frequency range [24]. Below 100 MHz, the two dominant noise sources are the $G-R$ noise and the $1/f$ noise, while the diffusion noise becomes significant when $G-R$ and $1/f$ noise vanish at higher frequencies. The $G-R$ noise is caused by fluctuaions in the number of free carriers and can be related to the presence of trap centers in the forbidden gap, while the physical origin of $1/f$ noise in semiconductor devices remains unknown as yet. The LF noise, usually measured as an equivalent noise voltage referred to the input gate, can be expressed as [25]

$$\overline{v_n^2} = 4kT\Delta f\left(\rho_0\frac{f_0}{f} + \sum_{r=1}^{n}\frac{\rho_r(\tau_r/\tau_0)}{1+(2\pi f\tau_r)^2}\right) \tag{24}$$

where ρ_0 is the $1/f$ noise equivalent gate resistance when $f = f_0$, ρ_r is a similar resistance for the rth component of the GR noise, τ_0 is a reference time constant, and τ_r the time constant for the trap causing GR noise. A typical evolution of $\overline{v_n^2}$ in HEMT's is presented in Fig. 7, which shows $G-R$ noise components superimposed on a background of $1/f$ noise. This is similar to the LF noise behavior of MESFET's.

The experimental study of the HEMT LF noise spectra [25]–[27] has clearly indicated several effects:

(i) The GR noise originates from (AlGa)As only and the noise magnitude is higher than that of the MESFET one.

(ii) A higher Al mode fraction enhances the trap concentration that causes the $G-R$ bulge near 10 kHz.

(iii) A close correlation exists between the amplitude of the room-temperature LF noise and the device properties at low temperature.

Therefore, the complex band structure of (Al,Ga)As and the multiple donor levels introduced by the dopant atoms [28] are the main causes of the observed strong LF noise. The use of low Al mole fraction (< 0.2) can reduce the amplitude of the GR noise, but is not well suited to provide high sheet carrier concentration and therefore high performance devices. However, it has been shown that the low-temperature parasitic effects (persistent photoconductivity, collapse, etc.) can be greatly reduced by spatially separating Al and the dopant atoms. This can be done using a superlattice [29] or an atomic planar doped layer [30]. These structures are then likely to present low LF noise and can be used for the realization of high-frequency oscillators with good spectral purity.

VII. High-Frequency Noise Measurement Techniques

A precise determination of the device noise performance is of primary importance in comparing various devices, validating the design of a low-noise device, and validating noise modeling. For this purpose, two different methods can be used: the conventional method and the least-squares fit of measured noise figures as a function of the input termination.

A. The Conventional Method

Fig. 8 shows a typical microwave transistor noise characterization system. The automatic noise-figure indicator provides the noise figure and gain of all the amplifier stages constituted by the bias networks, the tuners, and the device in the fixture. The main problem is then to deduce the noise figure F and associated G of the device using the measured F_m, G_m values.

In fact the noise figure of a cascade of noisy two-ports is given by the Friis formula:

$$F_m = F_1 + \frac{F-1}{G_1} + \frac{F_2-1}{GG_1}. \tag{25}$$

In our case, F_1 and G_1 are the noise figure and available gain of the input matching two-port constituted by the input bias, the input tuner, and half of the test fixture, while F_2 refers to similar components for the output (Fig. 9). Since the input and output matching two-ports are passive networks, $F_1 = 1/G_1$ and $F_2 = 1/G_2$ and (25) can be written as

$$F_m = \frac{F}{G_1} + \frac{1-G_2}{GG_1G_2} \tag{26}$$

or

$$F = G_1\left(F_m - \frac{1-G_2}{G_m}\right) \tag{27}$$

where $G_m = GG_1G_2$.

Expression (27) shows that an accurate determination of the device noise figure F needs an accurate determination of G_1. As shown by Strid [31], the popular back-to-back method for determining G_1 can be very inaccurate; therefore, it is preferable to calculate G_1 from S parameters

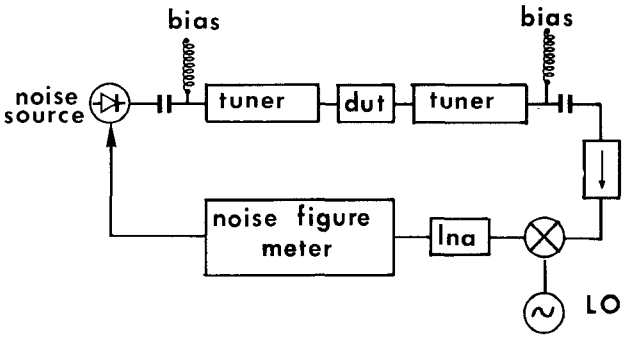

Fig. 8 Typical microwave transistor noise characterization system.

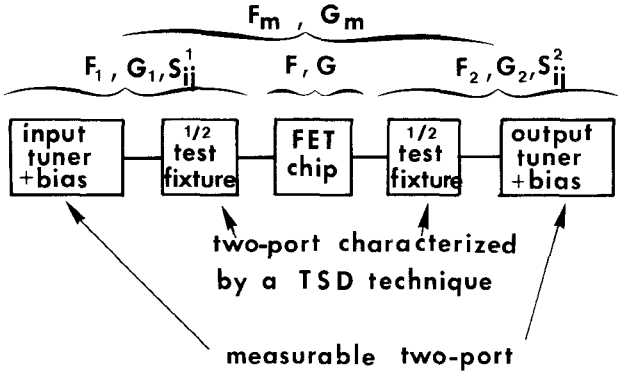

Fig. 9. Extraction of the device noise figure F and associated gain G from the measured values F_m and G_m.

that can be measured with a high accuracy. The S parameters (S^1_{ij}) of the whole input network are easily calculated from the S parameters of the input bias + tuner, which can be measured, and from the S parameters of the input half test fixture, which can be provided by a TSD technique [38]. Assuming an ideal generator impedance, we have

$$G_1 = \frac{|S^1_{21}|^2}{1-|S^1_{22}|^2}. \tag{28}$$

The determination of G_2 can be carried out in a similar way.

This method has several drawbacks:

(i) A long measurement time is required for seeking the minimum noise figure as well as for the S parameter measurements.

(ii) A minimum observed value F_m does not always provide the device minimum noise figure after the correction for the losses.

(iii) An additional measurement is needed for the noise resistance R_n (or noise conductance g_n) determination.

For these reasons, a more systematic method has been proposed [32].

B. The Noise Parameter Determination by Least-Squares Fit

Instead of randomly searching for the real minimum noise figure, another method is to measure the noise figure for different input reflection coefficients. Although four measurements are needed to determine the four unknowns

(F_{min}, R_n, Γ_{opt}) of the relation (29)

$$F = F_{min} + \frac{4R_n}{|1+\Gamma_{opt}|^2} \frac{|\Gamma_0 - \Gamma_{opt}|^2}{1-|\Gamma_0|^2} \quad (29)$$

where Γ_0 is the input reflection coefficient, it is better to perform seven or more measurements and then to determine the four noise coefficients by a least-squares fit of expression (29) [32], [33]. This technique reduces the derivation of the noise parameters to the solution of a four-linear-equation system [32]. A successive approximation technique has also been proposed to take into account the errors in the input reflection coefficient evaluation [34].

The major advantage of this measurement technique is the possibility of a fully automatic noise and gain characterization of a device [37], while its main drawback is the possibility of erroneous results or even results without physical meaning [36], especially at high microwave frequencies. These problem arise from the following causes:

(i) The computed results are highly sensitive to measurement errors in the case of a large noise resistance R_n [32].

(ii) The matrix of the four-linear-equation system which is to be solved can become singular for some values of the input termination [36].

(iii) The noise measurements are very sensitive to oscillations that can occur at low frequency, for which HEMT's are always potentially unstable. This major problem can be reduced if no tuner is used at the output of the DUT [37].

(iv) In the case of very low noise devices, the problem of input network losses is reduced but not suppressed.

For these different reasons, this method seems to be very well suited for systematic measurements in industrial laboratories rather than for measurements of high-performance devices at high frequency. Moreover, the published results concern mainly frequencies of operation lower than 12 GHz and devices providing rather high noise figures. Therefore, in the case of high-frequency (>18 GHz) noise figure determination, the conventional searching of F_{min} seems presently to be more accurate and more suitable, even if it is tedious. The recent possibility of accurate S parameter measurements up to 40 GHz, yielding accurate losses determination, confirms this assertion.

VIII. Conclusions

The general method yielding the HEMT noise parameters F_{min}, g_n, and Z_{opt} has been described. In order to consider the influence of the various parameters, different approximations have been carried out, and their results have been compared with experimental findings concerning high-performance devices. This analysis has shown that the gate noise and the correlation coefficient plays a prominant part in the noise parameter value. A comparison of the noise performance of both HEMT's and conventional MESFET's has shown that the HEMT superiority can be mainly related to the higher cutoff frequency and correlation coefficient.

Some particular aspects of the HEMT LF noise have then been discussed and structures with reduced LF noise have been proposed. Lastly, the two main experimental methods for determining the noise figure have been presented and their advantages and drawbacks have been discussed.

References

[1] H. Rothe and W Dahlke, "Theory of noisy fourpoles," *Proc. IRE*, vol. 44, pp 811–818, 1956.

[2] R. A. Pucel, H. A. Haus, and H. Statz, "Signal and noise properties of gallium arsenide field effect transistors," *advances in electronics and electron physics*, vol. 38, pp. 195–265, 1974.

[3] T. M. Brookes, "The noise properties of high electron mobility transistors," *IEEE Trans. Electron Devices*, vol. ED-33, no. 1, pp. 52–57, 1986.

[4] C. F Whiteside, G. Bosman, H. Morkoc, and W. F. Kopp, "The dc, ac, and noise properties of the GaAs:AlGaAs modulation-doped field effect transistor channel," *IEEE Trans. Electron Devices*, vol. ED 33 no. 10, pp. 1439–1445, 1986.

[5] A. Cappy, A. Vanoverschelde, M. Schortgen, C. Versnaeyen, and G. Salmer, "Noise modeling in submicrometer-gate two dimensional electron-gas field effect transistor," *IEEE Trans. Electron Devices*, vol ED 32, no. 12, pp. 2787–2795, 1985.

[6] B. Carnez, A. Cappy, R. Fauquembergue, E. Constant, and G. Salmer, "Noise modeling in sub-micrometer-gate FET's," *IEEE Trans. Electron Devices*, vol. ED 28, no. 7, pp. 784–789, 1981.

[7] A. van der Ziel, "Thermal noise in field effect transistor," *Proc. IRE*, vol. 50 pp. 1808–1812, 1962.

[8] A. van der Ziel, "Gate noise in field effect transistors at moderately high frequencies," *Proc. IRE*, vol. 51 pp. 461–467, 1963.

[9] D. Delagebeaudeuf, I. Chevrier, M. Laviron, and P. Delescluse, "A new relationship between the Fukui coefficient and optimal current value for low noise operation of field effect transistors," *IEEE Electron Device Lett.*, vol. EDL-6 no. 9, pp. 444–445, 1985.

[10] C. Moglestue, "A Monte Carlo particle study of the intrinsic noise figure in GaAs MESFET," *IEEE Trans. Electron Devices*, vol. ED-32 no. 10, pp. 2092–2096, 1985.

[11] F. M. Klaasen, "High-frequency noise of the function field-effect transistor," *IEEE Trans. Electron Devices*, vol. ED-14, no. 7, pp. 368–373, 1967.

[12] W. Beachhold, "Noise behavior of GaAs field-effect transistor with short gate length," *IEEE Trans. Electron Devices*, vol. ED-19 no. 5, pp. 674–680, 1972.

[13] C. H. Oxley and A. J. Holden, "Simple models for high-frequency MESFET's and comparison with experimental results," in *Proc. IEEE MOA*, June 1986.

[14] P C. Chao, S. C. Palmateer, P. M. Smith, V. K. Mishra, K. H. G. Duh, and J. C. M. Hwang, "Millimeter-wave low noise high electron mobility transistors," *IEEE Electron. Device Lett.*, vol. EDL-6, no. 10, pp. 531–533, 1985.

[15] B. Kim, H. Q. Tserng, and H. D. Shih, "Millimeter-wave GaAs FET prepared by MBE," *IEEE Electron. Device Lett.*, vol. EDL-6 pp. 1–2, 1985.

[16] P W. Chye and C. Huang, "Quarter-Micron low noise GaAs FET's," *IEEE Electron Device Lett.*, vol. EDL-3 pp. 401–403, 1982.

[17] J. Zimmermann, and Wu Yen, "Etude de la dynamique des electrons à deux dimensions dans les hétérojonctions," *Rev. Phys. Appl.*, to be published.

[18] H Fukui, "Design of microwave GaAs MESFET's for broad-band low noise amplifiers," *IEEE Trans. Microwave Theory Tech.*, vol. MTT-27, pp 643–650, 1979.

[19] S J. Lee and C. R. Crowell, "Parasitic source and drain resistance in high-electron-mobility transistors," *Solid-State Electron.*, vol. 28 no. 7, pp. 659–668, 1985.

[20] M. D. Feuer, "Two-layer model for source resistance in selectively doped heterojonction transistors," *IEEE Trans. Electron Devices*, vol. ED-32, no. 1, pp. 7–11, 1985.

[21] C. Versnayen, A. Vanoverschelde, A. Cappy, G. Salmer, and M. Schortgen, "Frequency dependence of source access resistance of heterojonction field-effect transistor," *Electron. Lett.*, vol. 21, no. 12 pp. 539–540, 1985.

[22] K. H. G. Duh, P. C. Chao, P. M. Smith, L. F Lester, and B. R. Lee, "60 GHz low noise high-electron mobility transistors," *Electron Lett*, vol. 22, no. 12, pp. 547–549, 1986.

[23] M. W. Pospiezalski, S. Weinreb, P. C. Chao, U. K. Mishra, S. C. Palmateer, P. M. Smith, and J. C. M. Huang, "Noise parameters and light sensitivity of low noise high electron mobility transistors at 300 and 12.5 K," *IEEE Trans. Electron Devices*, vol. ED-33 pp. 218–233, 1986.

[24] K. Kurokawa, "Noise in synchronized oscillators," *IEEE Trans. Microwave Theory Tech.*, vol. MTT-16, no. 4, pp. 234–240, 1968.

[25] S. M. Liu, M. B. Das, W. Kopp, and H. Morkoc, "Noise behaviour of 1 μm gate-length modulation-doped FET's from 10^{-2} to 10^{8} Hz," *IEEE Electron Device Lett.*, vol. EDL-6 no. 9, pp. 453–455, 1985.

[26] J. M. Dieudonne, M. Pouysegur, J. Graffeuil, and J. L. Cazaux, "Correlation between low-frequency noise and low temperature performance of two-dimensional electron gas FET's," *IEEE Trans. Electron Devices*, vol. ED-33 no. 5, pp. 572–575, 1986.

[27] L. Loreck, H. Dambkes, K. Heime, K. Ploog, and G. Weimann, "Deep level analysis in (AlGa)As-GaAs 2D electron gas devices by means of low frequency noise measurements," *IEEE Electron Device Lett.*, vol. ED-5 no. 1, pp. 9–11, 1984.

[28] E. F. Schubert and K. Ploog, "Shallow and deep donors in direct gap n type $Al_xGa_{1-x}As$:Si grown by molecular beam epitaxy" *Phy. Rev. B*, vol. 30, no. 12, pp. 7021–7029, 1984.

[29] T. Baba, T. Mizutani, and M. Ogawa, "Elimination of persistent photoconductivily and improvement in Si activation coefficient by Al spatial separation from Ga and Si in Al-Ga-As:Si solid system—A novel short period AlAs/n-GaAs superlattice," *Jap. J. Appl. Phys.*, vol. 22 no. 10, pp. L627–L629, 1983.

[30] S. Hiyamizu, S. Sasa, T. Ishikawa, K. Kondo, and H. Ishikawa, "A new hetero structure for 2 DEG system with a Si atomic-planar-doped AlAs-GaAs-AlAs quantum well structure grown by MBE," *Jap. J. Appl. Phys.*, vol. 24, pp. L431–L433, 1985.

[31] E. Strid, "Measurement of losses in noise-matching networks," *IEEE Trans. Microwave Theory Tech.*, vol. MTT-29, no. 3, pp. 247–252, 1981.

[32] R. Q. Lane, "The determination of device noise parameters," *Proc. IEEE*, vol. 57 pp. 1461–1462, 1969.

[33] G. Garuso and M. Sannino, "Computer aided determination of microwave two port noise parameters," *IEEE Trans. Microwave Theory Tech.*, vol. MTT 26, no. 9, pp. 639–643, 1978.

[34] M. Mitama and H. Katoh, "An improved computational method for noise parameter measurement," *IEEE Trans. Microwave Theory Tech.*, vol. MTT-27, no. 6, pp. 612–615, 1979.

[35] M. Sannino, "Computer aided simultaneous determination of noise and gain parameters of microwave transistors," in *Proc. European Microwave Conf.*, (Brighton, U.K.), pp. 692–695, 1979.

[36] M. Sannino, "On the determination of device noise and gain parameters," *Proc. IEEE*, vol. 67 no. 9, pp. 1364–1367, 1979.

[37] E. F. Calandra, G. Martines, and M. Sannino, "Characterization of GaAs FET's in terms of noise, gain and scattering parameters through a noise parameters test set," *IEEE Trans. Microwave Theory Tech.*, vol. MTT-32, no. 3, pp. 231–237, 1984.

[38] R. A. Speciale, "A generalization of the TSD network calibration procedure, coupling n port scattering parameter measurements affected by leakage errors," *IEEE Trans. Microwave Theory Tech.*, vol. MTT-25, no. 12 pp. 1100–1115, 1977.

[39] J. J. Berenz, K. Nakano, and K. P. Weller, "Low noise high electron mobility transistors," in *IEEE MTT-S Symp. Dig.*, pp. 83–86, 1984.

[40] P. R. Jay, H. Derewonko, D. Adam, P. Briere, D. Delagebeaudeuf, P. Delescluse, and J. F. Rochette, "Design of TEGFET devices for optimum low noise high frequency operation," *IEEE Trans. Electron Devices*, vol. ED-33, no. 5, pp. 590–594, 1986.

[41] K. Kamei, S. Hori, H. Kawasaki, K. Shibata, H. Mashita, Y. Ashizawa, "Low noise high electron mobility transistor," in *Proc. 11th GaAs and Related Compounds Conf.*, (Biarritz, France), 1984.

[42] H. Hida, K. Ohata, Y. Suzuki, and H. Toyoshima, "A new low noise AlGaAs:GaAs 2 DEG with a surface undoped layer," *IEEE Trans. Electron Devices*, vol. ED-33 no. 5, pp. 601–607, 1986.

[43] K. Tanaka, M. Ogawa, K. Togashi, H. Takakuwa, H. Ohke, M. Kanazuwa, U. Kato, and S. Watanabe, "Low-noise HEMT using MOCVD," *IEEE Trans. Electron Devices*, vol. ED-33 no. 12, pp. 2053–2058, 1986.

[44] K. Joshin, T. Mimura, M. Niori, Y. Yamashita, K. Kosmura, and J. Saito, "Noise performance of microwave HEMT," in *IEEE MTT-S Symp. Dig.*, pp. 563–565, 1983.

[45] M. Wolny, P. Chambery, A. Briere, and J. P. Andre, "Low noise high electron mobility transistor grown by MOVPE," in *Proc. High Speed Electronics Conf.* (Stockholm, Sweden), 1986, pp. 148–151.

✠

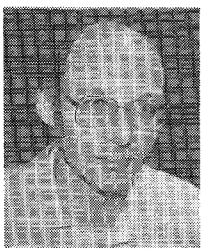

Alain CAPPY was born in Chalons sur Marne, France, on January 25, 1954. In 1977 he joined the Centre Hyperfrequences et Semiconducteurs at the University of Lille, France, and he received the Docteur en Electronique and Docteur es Sciences degrees from the University of Lille. His main research interests are semiconductor devices modeling, noise modeling in submicrometer-gate FET's and TEGFET's, and FET characterization techniques.

Dr. Cappy is a founder of the International GaAs Simulation Group.